# PENNSTATE
## 1855

# Applied Research Laboratory

# Acoustic Intensity Scattered from an Elliptic Cylinder

## G.C. Lauchle and K. Kim

Technical Memorandum
File No. 00-124
August 4, 2000

Copy No. _12_

**20000828 103**

# Acoustic Intensity Scattered from an Elliptic Cylinder

**G. C. Lauchle, K. Kim**
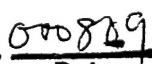
Technical Memorandum
File No. TM 00-124
August 4, 2000

**Never issued as IM**

Abstract:     A computational study is described where a 2-D elliptic cylinder is insonified by a plane, monochromatic acoustic wave. The elliptic cross section of the cylinder has a fineness ratio of 5:1, the incidence angle of the plane wave is 30° and 60° relative to the major axis of the ellipse, and $ka = 20$, where $a$ is the major axis of the elliptic cross section and $k$ is the acoustic wavenumber. The calculations are performed using the finite element method of solution for partial differential equations. The MATLAB® Partial Differential Equations Toolbox was used to formulate and solve the Helmholtz equation with reflection-free conditions imposed on the computational outer boundary, and rigid conditions imposed on the surface of the scatterer. Of particular practical interest in this study is the spatial distribution of the total active acoustic intensity, i.e., the sum of the incident and scattered intensity components. Active intensity amplitude, and the phase between pressure and particle velocity, are computed and compared to pressure amplitude only. The results show that there is significant phase distortion in the forward scattered direction that could be useful in localizing targets in active bi-static operations if $p$-$u$ type acoustic intensity probes were employed. The effects of reverberation on intensity measurements in active target localization systems are also discussed. This can have an effect on the phase results if the source is operating under steady-state conditions. If the source is operated with a short transient signal, the effect of reverberation is non-existent.

Approved for Public Release; Distribution Unlimited

Approved for publication

R. Stern          Date

# TABLE OF CONTENTS

# LIST OF FIGURES

# INTRODUCTION

Littoral ASW is an important thrust in the current Navy. Enabling capabilities include the detection, classification, and tracking of distant targets, and the characterization of the battle space. Traditionally, this is performed by rapid, covert deployment of surveillance systems, most of which use acoustic sensors and acoustic signal and information processing methodology. Pressure hydrophones are the standard sensor used in these applications. Acoustic intensity, on the other hand is the product of acoustic pressure and acoustic particle velocity. It is a vector quantity that describes the acoustic energy per unit area per unit time that is radiated from an acoustic source, or is scattered by an object insonified by that source. It is not a traditional measure in the underwater acoustics arena, primarily because there were no reliable means, until now, to measure it. Because state-of-the-art underwater acoustic intensity vector sensors can measure the real-time phase shifts between pressure and particle velocity, a whole new area of acoustic data interpretation is now available through use of these novel sensors. One application is to use these devices in passive DIFAR systems, where collocated pressure and acoustic velocity hydrophones already exist.

The use of intensity measurement methodology in active systems is not nearly as well understood at this time. Because it is very difficult to distinguish between the direct field and the scattered field in bi-static operations where the target is in the direct line between receiver and source, there is a need for research to determine whether intensity sensors offer any solution to this problem. The primary emphasis of the research described in this report is to determine, theoretically, the advantages, or disadvantages, of using underwater acoustic intensity sensors in active target localization scenarios. The issue is whether the acoustic intensity, determined by a direct measurement of the particle velocity, the pressure, and the phase between them, provides additional new information on the scattering characteristics of a target over that obtained from conventional pressure or acoustic velocity hydrophones used alone.

## I. PROBLEM STATEMENT

We use a rigid 2-D surface as the target. This surface is an elliptic cylinder that mimics a hydrofoil that may be attached to a submersible. The scattered pressure, particle velocity, and acoustic intensity are determined from numerical solutions of the Helmholtz equation. The MATLAB® Partial Differential Equations Toolbox, that utilizes the finite element method (FEM) of computation, is used for this exercise. We concentrate on the *total* acoustic intensity distributed throughout the field. This is the complex sum of the incident intensity from an arbitrarily located distant source and the intensity scattered from the surface. It would be representative of the intensity signal measured when the sound source is broadcasting a single-frequency wave under continuous, steady-state conditions.

We assume that a pressure-acoustic velocity (*p-u* type) intensity sensor [1] measures the field. These probes measure intensity *directly* and make no estimate of pressure or particle velocity using finite-difference solutions of either the continuity equation or the linearized Euler's equation, as is necessary in velocity-velocity *(u-u)* [2,3] and pressure-pressure *(p-p)* [4] probes, respectively. The phase between $p$ (acoustic pressure) and $u$ (acoustic particle velocity), or $p$ and $u \cdot dot$ (acoustic particle acceleration) [5] is always available. These two quantities are measured at the same point

in space using the probes under development at both Penn State and in an SBIR-supported industry (Acoustech Corp.). In a plane propagating wave field, the phase between pressure and velocity is $0°$, while in a reactive field, it is $90°$. Our goal is to determine what the phase is in a scattered field at various locations around the scatterer in both the near and farfields. Figure 1 shows a sketch of the problem considered.
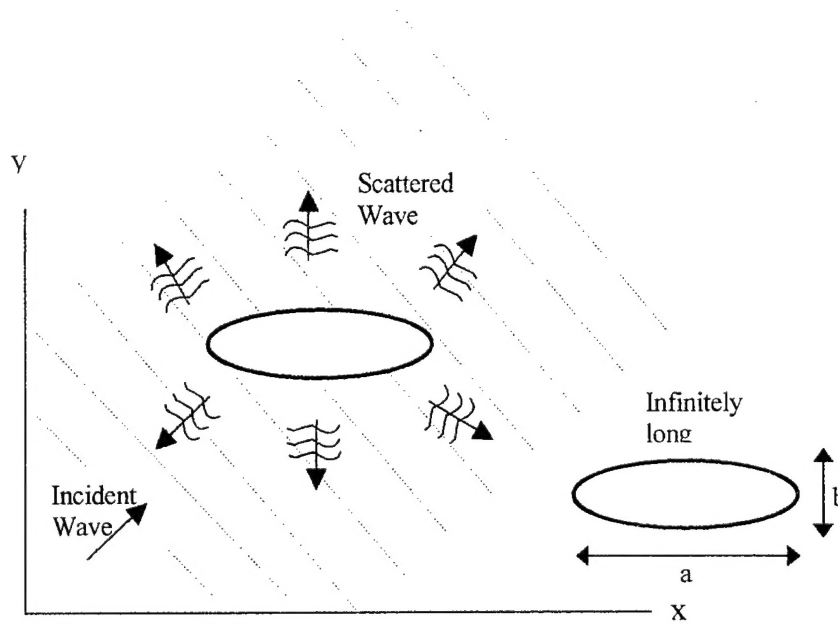


Figure 1        Scattering of a plane wave by a rigid elliptic cylinder.

## II. PROBLEM FORMULATION

The MATLAB® triangular mesh grid generator was used to create the scatterer and thousands of field points. We require at least 10 mesh points per acoustic wavelength. The triangular shaped mesh segments were jiggled so that the triangle quality factor,

$$q = \frac{4s\sqrt{3}}{h_1^2 + h_2^2 + h_3^2} \tag{1}$$

is greater than 0.6. Here, $h_i$ are the lengths of the sides of the triangles ($i = 1,2,3$), and $s$ is the area of the individual triangular mesh segments. Note that $q = 1$ for equilateral triangles. The final grid for the 5:1 elliptic cylinder is shown in Figure 2.

For acoustic radiation and scattering problems, the wave equation, which is hyperbolic, is solved:

2

$$\frac{\partial^2 p}{\partial t^2} - c^2 \nabla^2 p = 0 \qquad (2)$$

For time-harmonic excitation, $p(x,y,t) = p(x,y)e^{-i\omega t}$ this equation reduces to the Helmholtz equation, which is elliptic.

$$\nabla^2 p + k^2 p = 0 \qquad (3)$$

The MATLAB® PDE Toolbox allows either Equation (2) or (3) to be solved numerically; we solve (3), with $k = \omega/c$, where $c$ is the sound speed and $\omega$ is the radian frequency.

The incident wave is a plane wave propagating at angle $\theta$ to the x-axis:

$$p_i(x,y,t) = e^{i(\vec{k}\cdot\vec{r}-\omega t)} = e^{i(k_x x + k_y y - \omega t)} \qquad (4)$$

where $\left|\vec{k}\right|^2 = k_x^2 + k_y^2$, and $\theta = \cos^{-1}(k_x/\left|\vec{k}\right|)$. The elliptic cylinder is assumed rigid so that on the surface, $\vec{n} \cdot (\vec{\nabla} p) = \vec{n} \cdot (\vec{\nabla} p_i) + \vec{n} \cdot (\vec{\nabla} p_s) = 0$, where $p$ is the total acoustic pressure composed of the incident pressure and the scattered pressure, $p = p_i + p_s$. The vector $\vec{n}$ is the unit normal vector to the scattering surface. Because of the known form of the incident wave, we can express the gradient of the scattered pressure on the surface in the following form:
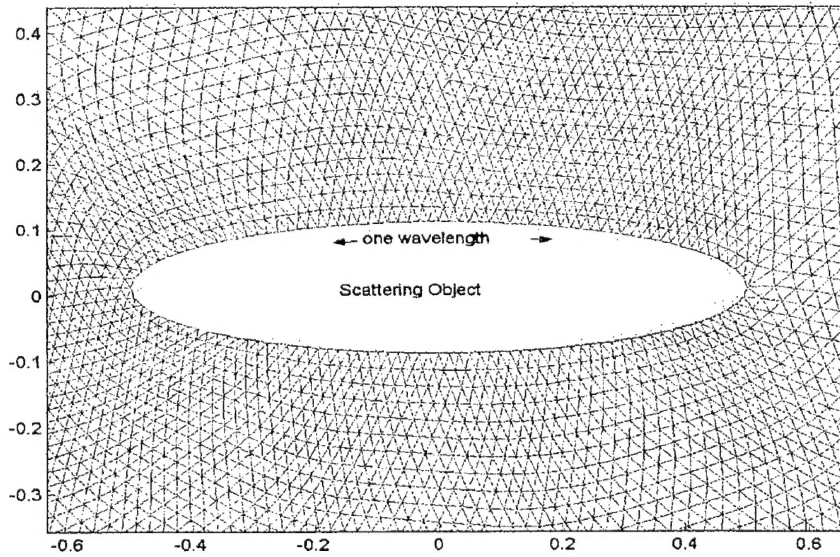


Figure 2    Computational domain and grid for solution of the scattering by an elliptic cylinder.

$$\vec{n} \cdot (\vec{\nabla} p_s) = -\vec{n} \cdot (\vec{\nabla} p_i) = -i(k_x n_x + k_y n_y)e^{i(k_x x + k_y y)} \qquad (5)$$

The outer boundaries of the computational grid must be chosen so that the waves pass through the boundary without reflection. We use the Sommerfeld radiation condition:

$$\frac{\partial p_s}{\partial t} + c\vec{n} \cdot \vec{\nabla} p_s = 0 \qquad (6)$$

where $\vec{n}$ is the unit normal to the outer boundary of the grid. Equation (6) is often referred to as the one-way wave equation because it allows waves to progress only in the positive n-direction. For harmonic time dependence, this becomes the generalized Neumann boundary condition:

$$\vec{n} \cdot \vec{\nabla} p_s = ikp_s \qquad (7)$$

To simplify the computations, and to maximize q, we chose the outer boundary normal to be approximately parallel to the normal of the scatterer.

The particle velocity is calculated using Euler's equation:

$$\rho \frac{\partial \vec{u}}{\partial t} = -\nabla p \qquad (8)$$

which is then conjugated and multiplied by one-half the pressure to get intensity:

$$\vec{I}(\vec{x}) = \frac{1}{2} p\vec{u}^* \qquad (9)$$

The real part of this expression is the *active* intensity, and the imaginary part is the *reactive* intensity.

The FEM modeling and coding was verified by comparing the numerical calculations with theoretically exact calculations. An infinitely long cylinder insonified by a plane wave was chosen for this verification. The analytical solution is [6]:

$$p_s(r, \phi) = \sum_{m=0}^{\infty} \left( -\varepsilon_m i^m \frac{J_{m-1}(ka) - J_{m+1}(ka)}{H_{m-1}^{(2)}(ka) - H_{m+1}^{(2)}(ka)} \right) H_m^{(2)}(kr) \cos(m\phi) \qquad (10)$$

where $\varepsilon_m = 1$ if $m = 0$, and 2 if $m > 0$, $J_m(ka)$ are Bessel functions, and $H_m^{(2)}(kr)$ are Hankel functions of the second kind. The unit amplitude incident pressure, in cylindrical coordinates is:

$$p_i(r, \phi) = 2\sum_{m=1}^{\infty} i^m J_m(kr) \cos(m\phi) + J_0(kr) \qquad (11)$$

where $\varphi$ is the angle between the direction of incidence and the radius vector from the cylinder axis to the field point, and $a$ is the radius of the cylinder. Figures 3 and 4 show the FEM solution and the exact solution, respectively. Here, kR = 3 and the series were summed to 15 terms. The comparison

4

is nearly perfect; therefore, the 2-D numerical solutions to the Helmholtz equation are considered to be verified.
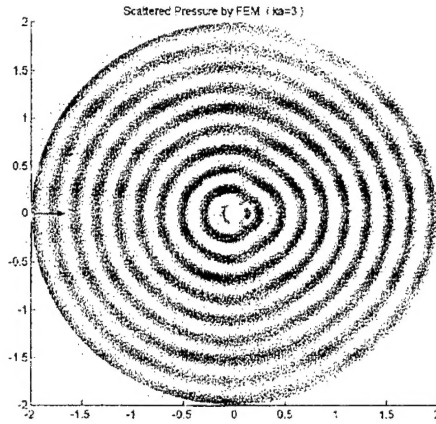


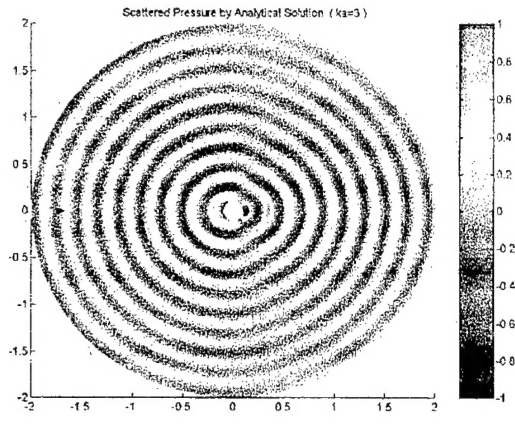Figure 3    Scattering by an infinite cylinder, FEM computation.

Figure 4    Scattering by an infinite cylinder, exact calculation.

## III. RESULTS

Calculations of the active intensity due to the scattering of a plane wave by a rigid, 2-D elliptic cylinder are presented in this section. The considered plane wave incidence angles are 30° and 60°. Figure 5 shows the computed total pressure field for ka = 20 and θ = 30°. The periodic color changes represent pressure magnitude changes as the compression and rarefaction parts of the acoustic wave pass various points in space. The computational boundaries are large enough so that the patterns shown near them represent far-field patterns. We note that the incident pressure field is described by the pattern in the vicinity of the arrow, which indicates the direction from the source. We might further note that the pattern in the forward scattered farfield is very similar to that of the incident field. That similarity makes the detection of the target difficult using pressure hydrophones as sensors. Calculations for the total pressure with θ = 60° are presented in Figure 6.

Turning our attention now to the computed intensity for the same situation as represented in Figures 5 and 6, Figures 7 and 8 show the magnitude of the active acoustic intensity field. The vectors show precisely how the acoustic energy interacts with the surface and diffracts around it to form a distorted intensity field nearly everywhere around the target. Of particular interest is how different the forward scattered intensity field is from the incident field. This means that an intensity measurement performed in the forward scattered direction may reveal target features not identified by acoustic pressure measurements alone. Although forward scattered highlights appear in the intensity field plots of Figures 7 and 8, they are actually "lowlights" because the magnitudes are smaller than that of the incident intensity, i.e., the forward scattered intensity reveals a strong shadow region.

Total Pressure (ka=20,a=1,b=0.2.angle=30)



Figure 5      Total acoustic pressure scattered by an elliptic cylinder. The source is situated in the lower left as indicated by the arrow at $\theta = 30°$.

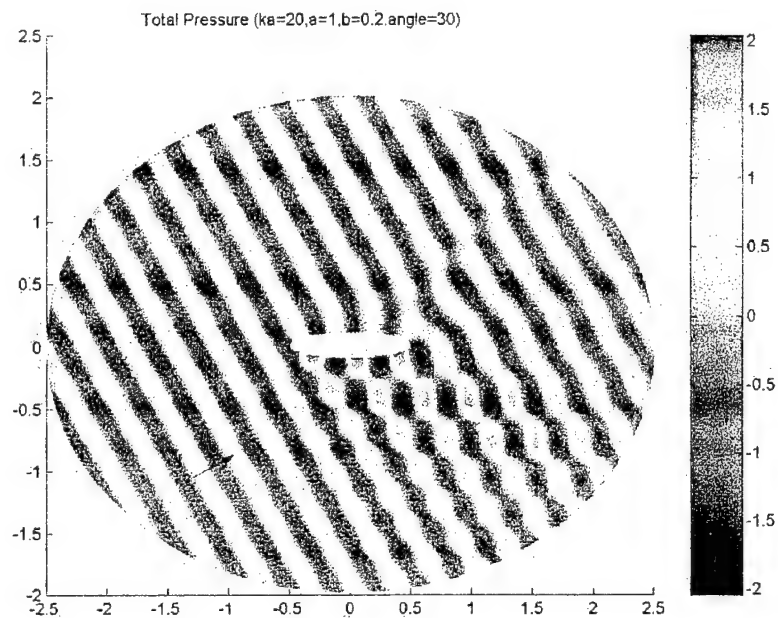Total Pressure ( ka=20, a=1,b=0.2,angle=60 )



Figure 6      Total acoustic pressure scattered by an elliptic cylinder. The source is situated in the lower left as indicated by the arrow at $\theta = 60°$.

6

Figure 7    Total active acoustic intensity scattered by an elliptic cylinder. The source is situated in the lower left as indicated by the origin of the vectors; $\theta = 30°$.
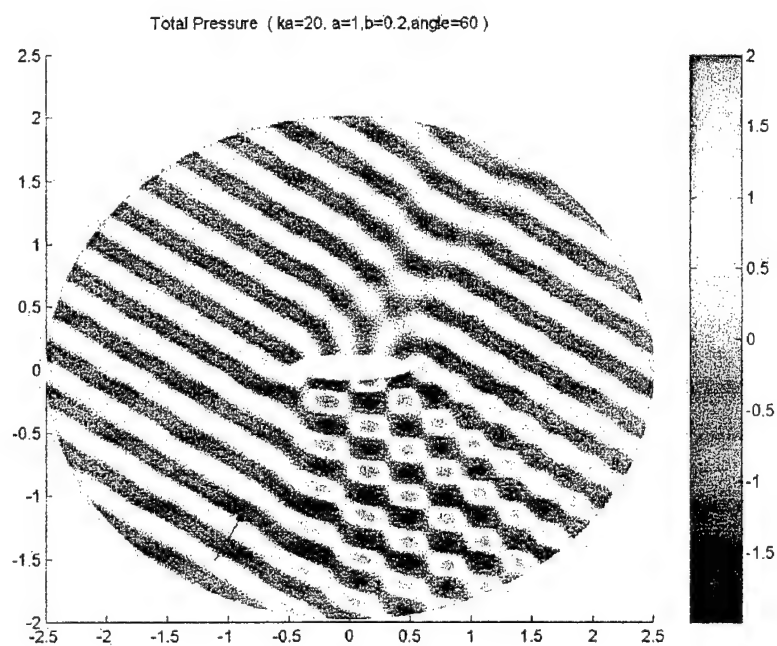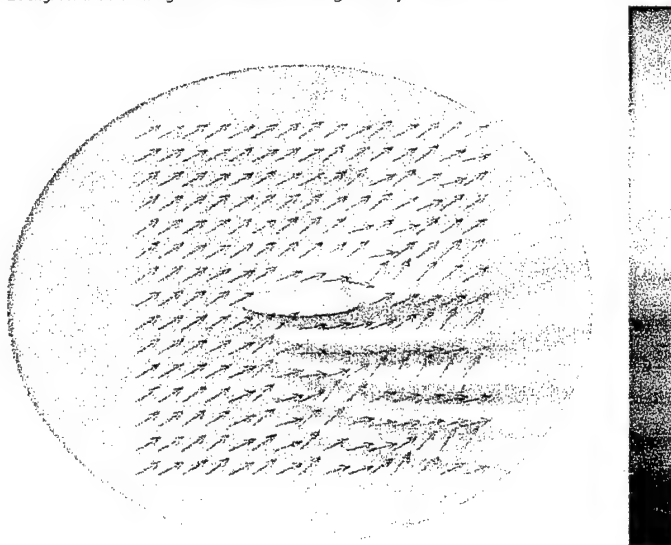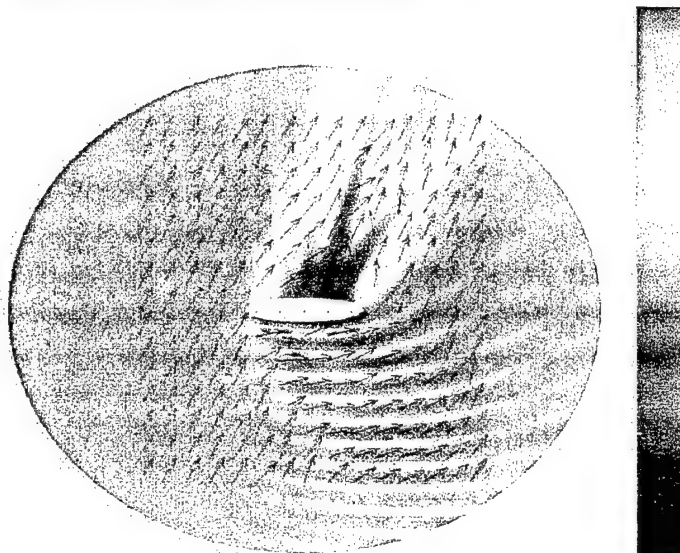
Figure 8    Total active acoustic intensity scattered by an elliptic cylinder. The source is situated in the lower left as indicated by the origin of the vectors; $\theta = 60°$.

7

The beam pattern expresses far-field magnitude in a polar format. The intensity beam pattern shows little more information than the beam pattern for the total acoustic pressure, e.g., Figure 9. Thus, simply measuring the *magnitude* of the active acoustic intensity in the farfield may not provide any advantage over measuring pressure (or particle velocity) alone. The important information is in *the phase* between the pressure and particle velocity.

Beam Pattern of Total Pressure and Radial Active Intensity in dB
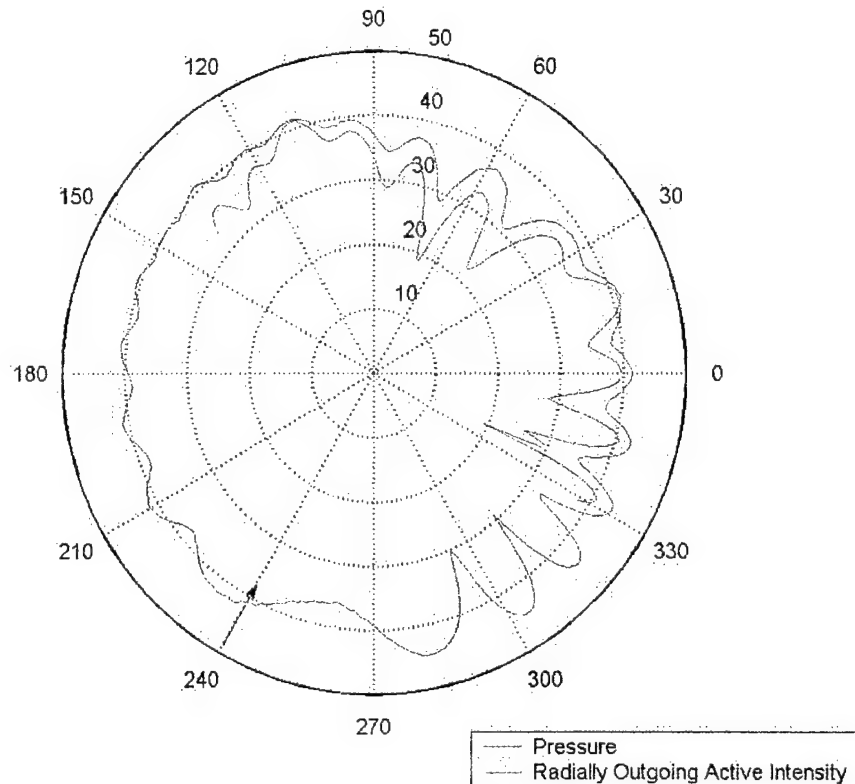


Figure 9    Beam patterns for the magnitude of the active intensity in the forward scattered directions compared to that of the total pressure; θ = 60°.

Figures 10 and 11 show the phase (radians) between the x-component of the acoustic velocity and the pressure at all field points around the scatterer insonified at 30° and 60°, respectively. The phase of the incident wave is simply kr which grows linearly with distance, r. The plot shows this linear growth as a sawtooth wave because the range of the phase is bounded between (-π,π). A remarkable deviation from the sawtooth pattern is evident in the forward scattered direction. This phase distortion should be easy to measure with a *p-u* or a *p-u dot* underwater acoustic intensity probe. Figures 12 and 13 show the phase between the y-component of particle velocity and the pressure. Again, significant phase distortion is evident in the forward scattered direction.

8

Phase between Pressure and Velocity in x-direction (ka=20,a=1,b=0.2,angle=30)

Figure 10    Phase between the x-component of particle velocity and acoustic pressure at collocated points in space during the scattering of a plane wave at 30° to an elliptic cylinder.

Phase between Pressure and Velocity in x-direction ( ka=20,a=1,b=0.2,angle=60)

Figure 11    Phase between the x-component of particle velocity and acoustic pressure at collocated points in space during the scattering of a plane wave at 60° to an elliptic cylinder.

Phase between Pressure and Velocity in y-direction (ka=20,a=1,b=0.2,angle=30)



Figure 12    Phase between the y-component of particle velocity and acoustic pressure at collocated points in space during the scattering of a plane wave at 30° to an elliptic cylinder.

Phase between Pressure and Velocity in y-direction ( ka=20,a=1,b=0.2,angle=60)
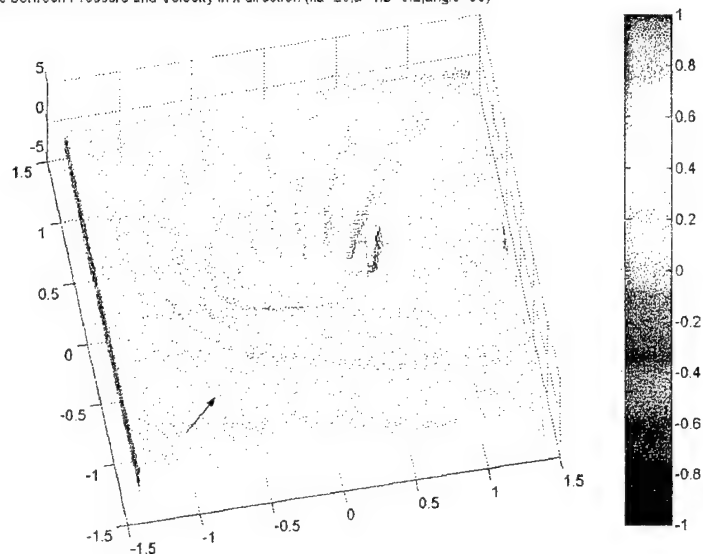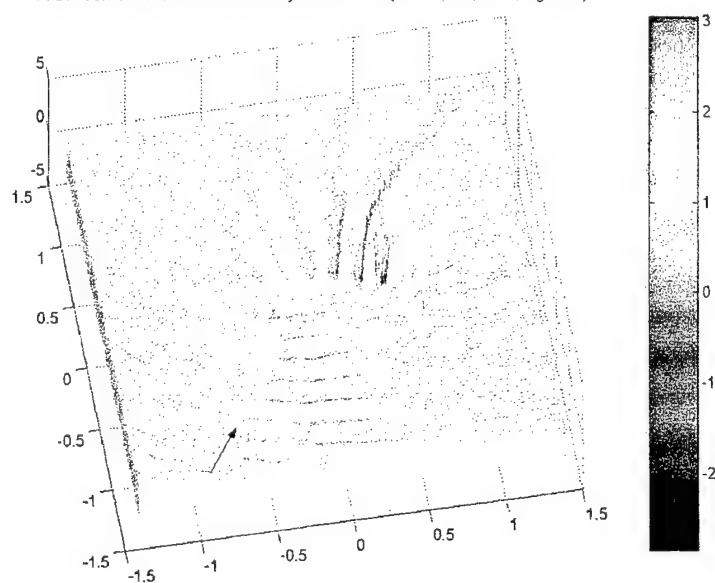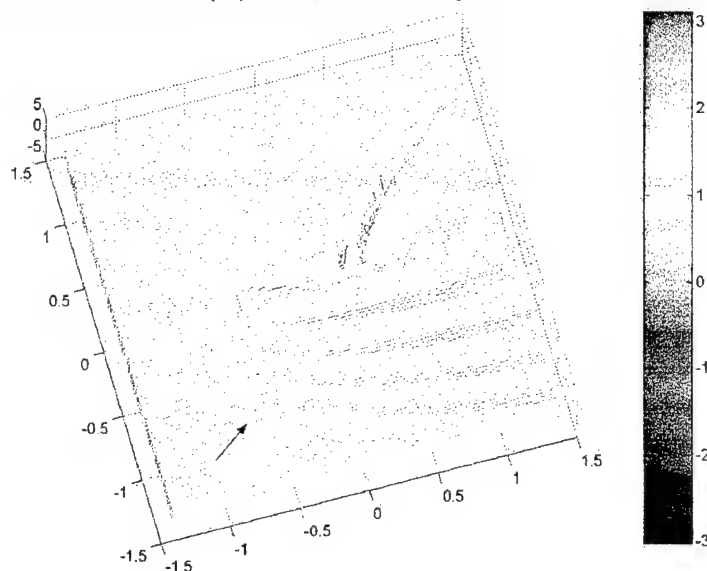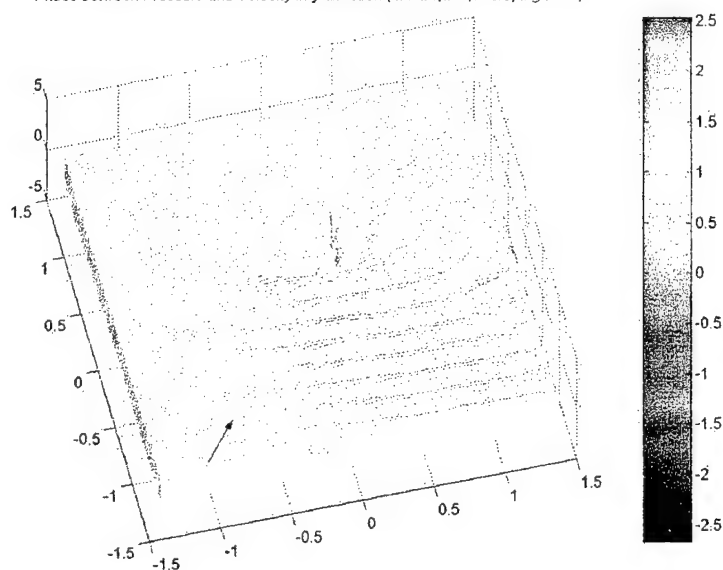


Figure 13    Phase between the y-component of particle velocity and acoustic pressure at collocated points in space during the scattering of a plane wave at 60° to an elliptic cylinder.

10

## A. Reverberation Effects

Active and reactive sound intensity measurements in reverberation chambers has been of interest to noise control engineers ever since the two-microphone method was invented in the early 1970's. Jacobsen [8], for example, has conducted considerable research on this topic and has derived equations for the coherence function between particle velocity and acoustic pressure in diffuse, reverberant fields. The field is assumed to be created by a steady-state source driven at a single frequency, $\omega$. The reflecting environment causes multi-path propagation. The signal that eventually reaches the receiver is composed of many plane waves originating from numerous locations. The amplitudes and point-of-origin of these waves are treated as random variables by Jacobsen. The resulting coherence function for two pressure signals obtained from two hydrophones separated by distance d is:

$$\gamma_{pp}^2 = \left( \frac{\sin kd}{kd} \right)^2 \tag{12}$$

Figure 14 shows a plot of Equation (12) where the two hydrophone separation distance is expressed in acoustic wavelengths.
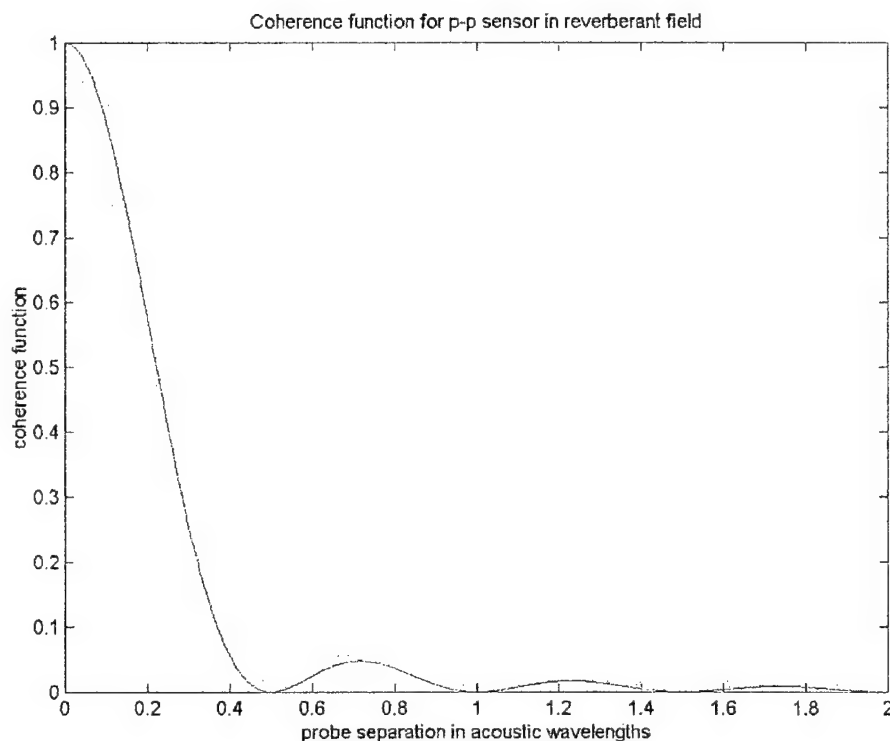


Figure 14    Coherence function between two pressure sensors in a reverberant field.

11

Clearly, from this equation and the plotted result, one can conclude that a *p-p* type intensity probe will show a large coherence in a reverberant field if *d* is small. The coherence (and the intensity) will be zero at the sinc function's first zero, which is when $d = \lambda/2$. The hydrophones would need to be separated by at least that amount in order to discriminate against reverberant background noise effects.

The coherence function for a *p-u* type intensity probe is:

$$\gamma_{pu}^2 = 3\left( \frac{\sin kd - kd \cos kd}{k^2 d^2} \right)^2 \tag{13}$$

This equation is useful for calculating the coherence due to reverberation between a pressure sensor and an acoustic velocity sensor separated by distance *d*. For the *p-u* probes under development at Penn State and Acoustech Corp., $d = 0$, and the coherence is zero. The intensity due to a diffuse reverberant background noise field sensed with this type of probe would also be zero. Figure 15 is a plot of Equation (13).



Figure 15      Coherence function between particle velocity and acoustic pressure in a reverberant field.

12

## IV. CONCLUSIONS
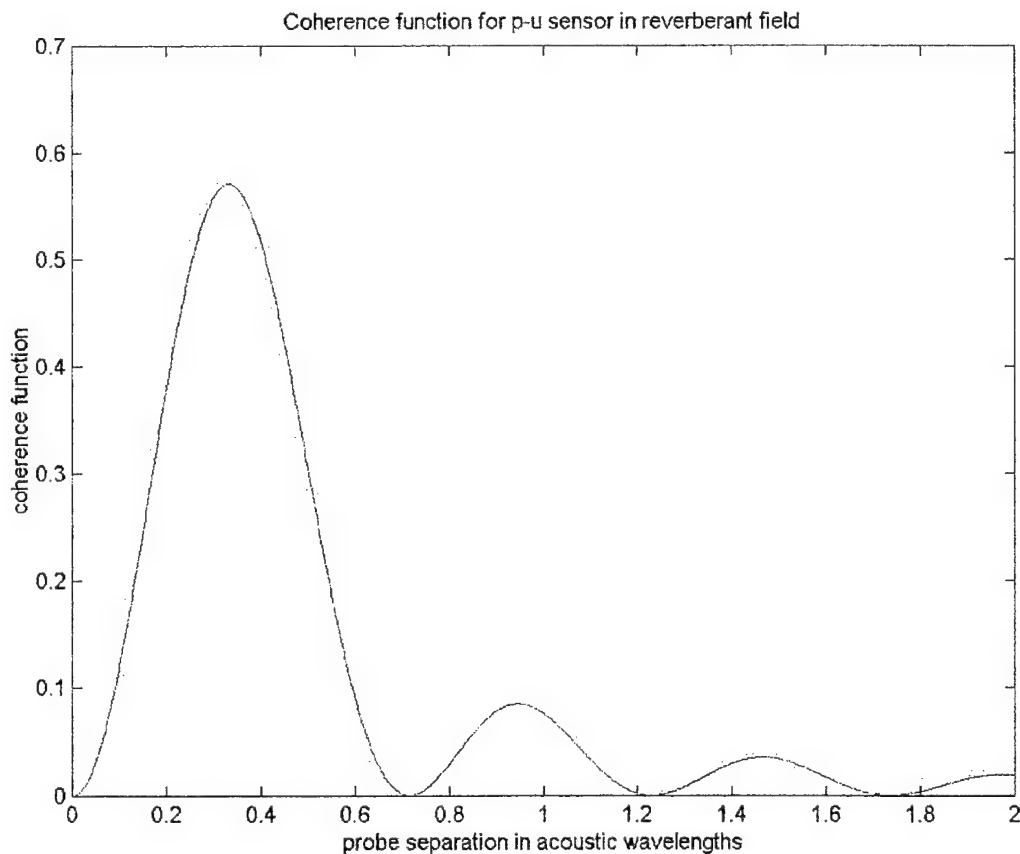
We have presented here numerical calculations of the acoustic scattering of plane waves by a rigid, 2-D elliptic cylinder. The particle velocity and pressure are computed and combined to form the active intensity. The interpretation of these results in terms of using intensity sensors in active systems is as follows:

- Under steady-state pure tone source excitation *in a reverberation-free environment*, the total (incident + scattered) active intensity field contains valuable information in the phase between particle velocity and acoustic pressure. In the forward scattered direction, this phase fluctuates rapidly with location suggesting that a target could be easily identified in this direction using a *p-u* type intensity probe.

- However, if the sound source is driven with a steady-state pure tone *in a reverberant environment*, the wave will eventually reverberate in the medium and the intensity measured with a collocated *p-u* probe will be zero everywhere. The phase distortions due to a particular scatterer, like those noted in Figures 10-13, may be masked by the reverberant effects. *A continuous, steady-state source signal should therefore be avoided in reverberant fields.*

- If the level of *ambient diffuse background noise* is comparable to, or larger than, the level produced by the active source, and if the source is driven *impulsively*, the background noise will not degrade the performance of an intensity measurement of the scattered field. In this case, it is assumed that the forward scattered path is the shortest path, and the phase distortions observed in Figures 10-13 should be easily identified. *An impulsive source signal should be used in reverberant fields together with p-u type intensity sensors.*

# REFERENCES

1. Gabrielson, T. B., J. F. McEachern, and G. C. Lauchle, "Underwater Acoustic Intensity Probe," U. S. Patent #5,392,258, Feb. 21, 1995.

2. McConnell, J. A., G. C. Lauchle, and T. B. Gabrielson, "Two-Geophone Underwater Acoustic Intensity Probe," Invention Disclosure dated 21 September 1995 (patent application submitted by U.S. Navy).

3. Bastyr, K. J., G. C. Lauchle, J. A. McConnell. Development of a Velocity Gradient Underwater Acoustic Intensity Sensor. *J. Acoust. Soc. Am.* **106**: 3178-3188 (1999).

4. Ng, K. W., "Acoustic Intensity Probe," U. S. Patent #4,982,375, Jan. 1, 1991.

5. Lauchle, G. C., T. B. Gabrielson, and J. A. McConnell, "Underwater Acoustic Vector Sensor," Penn State University Patent Disclosure No. 1974, 10 August 1998.

6. Skudrzyk, E. *Foundations of Acoustics: Basic Mathematics and Basic Acoustics* (Springer-Verlag, New York and Wien, 1971).

7. Jacobsen, F. The Diffuse Sound Field. The Acoustic Laboratory, The Technical University of Denmark, Report no. 27 (1979).

**DISTRIBUTION LIST FOR ARL PENN STATE TM 00-124 BY G. C. Lauchle and K. Kim, dated August 4, 2000.**

Commander
Office of Naval Research
800 N. Quincy Street
Arlington, VA 22217-5660
Attn: J. F. McEachern, Code 321SS
Copy No. 1

Office of Naval Research
Attn: Jan Lindberg, Code 321SS
Copy No. 2

Office of Naval Research
Attn: Roy Elswick, Code 321SS
Copy No. 3

Office of Naval Research
Attn: Ken Dial, Code 321SS
Copy No. 4

Office of Naval Research
Attn: Patrick Purtell, Code 334
Copy No. 5

Office of Naval Research
Attn: K. Ng, Code 333
Copy No. 6

Office of Naval Research
Attn: S. Lekoudis, Code 333
Copy No. 7

Office of Naval Research
Attn: G. Jebsen, Code 334
Copy No. 8

Office of Naval Research
Attn: E. Rood, Code 334
Copy No. 9

DARPA
3701 N. Fairfax Drive
Arlington, VA 22203-1714
Attn: James McMichael
Copy No. 9

Naval Air Warfare Center-Aircraft Div.
22347 Cedar Point Road - Unit 6
Code 4.5.5.4, Building 2185, Suite 1144
Patuxent River, MD 20670-1161
Attn:   Gordon Marshall
Copy No. 10

Director
Naval Research Laboratory
Washington, DC 20375
Copy No. 11

Defense Technical Documentation Center
8725 John J. Kingman Road
Suite 0944
Fort Belvoir, VA 22060
Copy Nos. 12 & 13

Office of Naval Research
5636 South Clark Street
Room 208
Chicago, IL 60605
Attn: David Wyner
Copy No. 14

Acoustech Corporation
P.O. Box 139
State College, PA 16804
Attn: J. A. McConnell
Copy No. 15

Naval Undersea Warfare Center-Division
Newport
1176 Howell Street
Newport, RI 02841-5047
Attn: Benjamin Cray, Code 2133
Copy No. 16

Naval Surface Warfare Center
Carderock Division
9500 MacArthur Boulevard
West Bethesda, MD 20817-5700
Attn: T. Farabee, Code 7250
Copy No. 17

Naval Surface Warfare Center
Carderock Division
Attn: W. K. Blake
Copy No. 18

Naval Sea Systems Command
2531 Jefferson Davis Highway
Arlington, VA 22242-5160
Attn: Jim Fein
Copy No. 19

CNO Executive Panel
4401 Ford Avenue
Alexandria, VA 22302-0268
Attn: Scott Littlefield
Copy No. 20

Naval Undersea Warfare Center Division,
Newport
1176 Howell Street
Newport, RI 02841-5047
Attn: P. J Lefebvre, Bldg. 990/5
Copy No. 21

Naval Undersea Warfare Center Division,
Newport
Attn: B. E. Sandman, Code 213
Copy No. 22

Naval Undersea Warfare Center Division,
Newport
Attn: R. Philips, Code 8233
Copy No. 23

Naval Undersea Warfare Center Division,
Newport
Attn: F. M. Cancilliere, Bldg. 990/5
Copy No. 24

Boston University
College of Engineering
110 Cummington Street
Boston, MA 02215
Attn: M. S. Howe
Copy No. 25

Boston University
College of Engineering
110 Cummington Street
Boston, MA 02215
Attn: A. D. Pierce
Copy No. 26

The Pennsylvania State University
134 Materials Research Laboratory
University Park PA 16802
Attn: K. Uchino
Copy No. 27

The Pennsylvania State University
134 Materials Research Laboratory
University Park PA 16802
Attn: L. E. Cross
Copy No. 28

The Pennsylvania State University
134 Materials Research Laboratory
University Park PA 16802
Attn: R. E. Newnham
Copy No. 29

The Pennsylvania State University
157a Hammond Building
University Park PA 16802
Attn: Gary Koopmann
Copy No. 30

The Pennsylvania State University
Graduate Program in Acoustics
P.O. Box 30
State College, PA 16804-0030
Attn: A. A. Atchley
Copy No. 31

Graduate Program in Acoustics
Attn: Vic Sparrow
Copy No. 32

Graduate Program in Acoustics
Attn: Kang Kim
Copy No. 33

Graduate Program in Acoustics
Attn: G. C. Lauchle
Copy No. 34

Graduate Program in Acoustics
Attn: W. Thompson, Jr.
Copy No. 35

Graduate Program in Acoustics
Attn: Sewon Park
Copy No. 36

Graduate Program in Acoustics
Attn: Jiri Tichy
Copy No. 37

The Pennsylvania State University
The Applied Research Laboratory
P.O. Box 30
State College, PA 16804-0030
Attn: L. R. Hettche
Copy No. 39

ARL Penn State
Attn: R. Stern
Copy No. 39

ARL Penn State
Attn: C. H. Brickell
Copy No. 40

ARL Penn State
Attn: D. L. Bradley
Copy No. 41

ARL Penn State
Attn: M. L. Billet
Copy No. 42

ARL Penn State
Attn: T. B. Gabrielson
Copy No. 43

ARL Penn State
Attn: Y.-Fan Hwang
Copy No. 44

ARL Penn State
Attn: H. J. Gibeling
Copy No. 45

ARL Penn State
Attn: R. C. Marboe
Copy No. 46

ARL Penn State
Attn: E. G. Liszka
Copy No. 47

ARL Penn State
Attn: D. E. Capone
Copy No. 48

ARL Penn State
Attn: T. A. Brungart
Copy No. 48

17

ARL Penn State
Attn: C. R. Zentner
Copy No. 49

ARL Penn State
Attn: F. W. Symons
Copy No. 50

ARL Penn State
Attn: W. J. Hughes
Copy No. 51

ARL Penn State
Attn: D. C. Swanson
Copy No. 52

ARL Penn State
Attn: ARL Library
Copy No. 53

ARL Penn State
Attn: GTWT Library
Copy No. 54